

1506. Analysis, realization and experiment of Lamb wave phased arrays for damage detection and imaging in carbon composite structures

Yajie Sun¹, Sai Ji²

¹Jiangsu Collaborative Innovation Center on Atmospheric Environment and Equipment Technology, Nanjing University of Information Science and Technology, No. 219 Ningliu Road, Nanjing, 210044, China

^{1,2}Jiangsu Engineering Center of Network Monitoring, Nanjing University of Information Science and Technology, No. 219 Ningliu Road, Nanjing, 210044, China

¹Corresponding author

E-mail: ¹syj@nuist.edu.cn, ²jisai@nuist.edu.cn

(Received 4 June 2014; received in revised form 16 July 2014; accepted 30 July 2014)

Abstract. Phased array theory is utilized in the unmanned aerial vehicle (UAV) wing box to identify the damage in the structure. The phased array theory has been adapted to Lamb wave propagation to improve the detection ability of local defects in the complex composite structure. The validity of the proposed method is demonstrated by experimental research in which input signals exerted at piezoelectric (PZT) actuators/sensors on the UAV wing box are successfully reconstructed by using the phased array method. The recognition result is shown on a mapped image. The original mapped image uses gray level transformation method to enhance the image identifiable degrees. And the time of arrival of the Lamb wave signal is calculated by Shannon Wavelet. The experiments is done on carbon composite structure using one dimensional PZT linear sensors array exemplifies that phased array theory well utilized in scanning and detecting the damage and the screw loosening in the structure. The original image is processed by the gray level transformation to improve the contrast and the recognition.

Keywords: carbon composite, phased array, structural health monitoring (SHM), image enhancement, Shannon wavelet, time of arrival (TOA).

1. Introduction

In order to improve safety and reliability, and to reduce maintenance costs of aerospace structures, development of efficient damage detection and localization techniques is essential [1-4]. Lamb wave can propagate a long distance in plate-like and shell-like structures [5-8]. Hence, structural health monitoring (SHM) [9-13] based on Lamb wave has emerged as a promising technique by using piezoelectric (PZT) actuators/sensors to generate/receive the signals for monitoring the structural damage. The SHM technology is different from the nondestructive examination (NDE) [14] that uses the damage detection strategies to monitor the structural state in real time.

Phased array is an effective damage detection and assessment method in the Lamb wave based SHM system. Comparing to the single sensor identification [15-16], the Lamb wave phased array takes advantage of beam steering to improve the sensitivity. The beam steering of Lamb wave is well controlled to the desired directions by phased array theory. When the wave beam encounters damage in the structure, it generates reflected signal. Previous scholars did a lot of research on phased array based inspection of thin wall structures [17-25]. These researches are not applied on a practical application of engineering.

In this paper, the Lamb wave phased array theory is applied in the structural health monitoring of UAV wing box to identify the damage in the structure. The identification result is shown on the mapped image. The gray level transformation method is used to improve the quality and the contrast of the original damage image. The Lamb wave phased array theory based damage identification and imaging method is verified by using one dimensional PZT linear sensors array

to scan and detect the damage and the screw loosening in the carbon composite structures. Meanwhile, the Shannon wavelet is used to calculate the time of arrival of the signals.

2. Phased array based monitoring and imaging theory

Ultrasonic phased array transducer consists of several piezoelectric sensors arranged in a linear array that are independently activated in a sequential manner to scan a certain range of the structure. The signal excited by these PZT sensors array interferes each other in space to form the wave beam-steering focusing on a certain direction. The superposition of ultrasonic wave takes shape in a new wave-front by controlling the phase delay of each excitation signal emitting by PZT array, which is equivalent to changing the location of the transducer. The beam-steering radiated by the PZT array is accordingly changed. And the same rule is implemented in reception of reflection wave. All the signals in the same direction received by PZT array are synthesized and the synthetic signals are shown on the mapped image. Therefore, the ultrasonic phased array can effectively control the direction of wave beam-steering by controlling the phase delay of excitation and reception signal to scan the structure.

Far-field phased array principle is shown in Fig. 1. The PZT linear array consists of M PZT elements with each PZT element acting as an omni-directional transmitter and receiver. The PZT elements in the array are equally spaced at the distance d . The diameter of the PZT element is d_1 . The coordinate system origin is set to the middle point of the PZT array and the 0° direction is consistent with the alignment of the array. The coordinate in Cartesian coordinate system of i th PZT element is $(x_i, 0)$, $i = 0, \dots, M - 1$, where $x_i = [i - (M - 1)/2]d$.

The phased array principle is applied to generate and receive Lamb waves. For a far-distance point $P(r, \theta)$, the distance r from point P to coordinate system origin is assumed much longer than the PZT element spacing d . Because $d \ll r$, the rays connecting the point P with the sensors can be considered with a parallel fascicle of θ . Coordinate system origin is acted as a reference point. For the i th PZT element, the distance from the point P to the sensor will be shorted by $\xi_i(\theta) = x_i \cos \theta$. If all the PZT elements are excited simultaneously, the signal from the i th PZT element will arrive at point P quicker by $\delta_i(\theta) = x_i \cos(\theta)/c$. Where c is the Lamb wave group speed traveling in the structure. The total signal received at point P will be:

$$S_p(t) = K_1 \sum_{i=0}^{M-1} S_e \left(t - \frac{r}{c} + \delta_i(\theta) \right), \quad (1)$$

where K_1 is the amplitude attenuation coefficient which the signal travelling from PZT to point P , S_e represents excitation signal, and r/c is the time due to the travel distance between the coordinate system origin and the point P . Here wave-amplitude conservation is assumed.

If the PZT elements are not excited simultaneously, but with specific time delays $\Delta t_i(\theta)$ for each PZT element, the total signal received at point P will be:

$$S_p(t) = K_1 \sum_{i=0}^{M-1} S_e \left(t - \frac{r}{c} + \delta_i(\theta) - \Delta t_i(\theta) \right). \quad (2)$$

If $\Delta t_i(\theta) = \delta_i(\theta)$, Eq. (2) becomes:

$$S_p(t) = K_1 M S_e \left(t - \frac{r}{c} \right). \quad (3)$$

In this case, the specific time delay for each PZT element is:

$$\Delta t_i(\theta) = \frac{x_i \cos \theta}{c} = \frac{\left(i - \frac{M-1}{2}\right) d \cos \theta}{c} \tag{4}$$

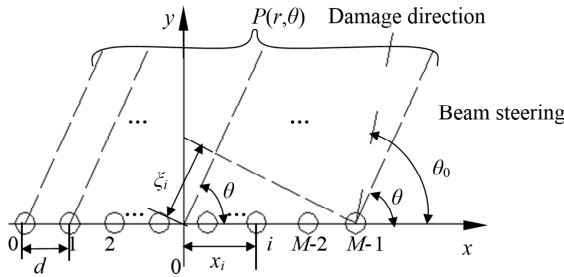


Fig. 1. Principle of phased array based structural health monitoring

The signal amplitude increases M times in comparison with a single PZT element. The signal-to-noise ratio (SNR) is enhanced. If $\Delta t_i(\theta) = \delta_i(\theta) = x_i \cos(\theta)/c$, the signal wave-front takes place at angles θ that is achieved by specific time delays of the exciting signals of the sensors in the linear array.

According to the principle of reciprocity, the receiving process is consistent with exciting process under the same conditions. The point $P(r, \theta)$ acts as a new wave source reflecting the signal to all the PZT elements. The signal arrives the i th PZT element quicker by $\delta_i(\theta) = x_i \cos(\theta)/c$. Its expression is:

$$S_i(t) = K_2 S_p \left(t - \frac{r}{c} + \delta_i(\theta) \right), \tag{5}$$

where K_1 is the amplitude attenuation coefficient which the signal travelling from point P to PZT.

The total signal received at all PZT elements from the point P will be:

$$S(t) = K_1 K_2 M \sum_{i=0}^{M-1} S_e \left(t - \frac{2r}{c} + \delta_i(\theta) \right). \tag{6}$$

Hence, with specific time delays $\Delta t_i(\theta) = \delta_i(\theta)$ for each PZT element, the signal reaches to all of the PZT elements at the same time. Its expression is:

$$\begin{aligned} S(t) &= K_1 K_2 M \sum_{i=0}^{M-1} S_e \left(t - \frac{2r}{c} + \delta_i(\theta) - \Delta t_i(\theta) \right) = K_1 K_2 M^2 S_e \left(t - \frac{2r}{c} \right) \\ &= K M^2 S_e \left(t - \frac{2r}{c} \right), \end{aligned} \tag{7}$$

where, $K = K_1 K_2$, K is the total amplitude attenuation coefficient.

Assume that damage exists at angle θ_0 and distance R in the structure. The signals scan the structure in increasing angles θ and the PZT elements receive the largest reflection signal from the damage when $\theta = \theta_0$.

By analyzing the signal in the damage direction, the distance R of the damage can be calculated as:

$$R = \frac{c\tau}{2}, \tag{8}$$

where τ is the time of arrival of the signal in the damage direction.

In conclusion, the damage location is achieved by the scanning direction and the calculating distance.

Taking the signal amplitude as a parameter, the sensing signal in the scanning angle is described in the mapped image because the signal amplitude is the function of the distance and the direction. The signal amplitude can be described on distance-direction two-dimensional plane in the gray form to get the mapped image. Gray-scale in the mapped image from dark to light corresponds to the amplitude from low to high. The highlight of the mapped image is the damage location in the structure.

The sensing signal collected in structure health state is acted as a reference signal. And the signal collected in structure damage state is compared with the reference signal to get the damage scattered signal in each direction. Then the time delay is added to the damage scattered signals. After time delay, the damage scattered signals in the same direction is cumulated to get the synthetic signal. The cumulative signal is described in the mapped image. Each point pixel of the mapped image is the synthetic signal normalized amplitude. The location in the mapped image of the synthetic signal is calculated by:

$$\begin{cases} x_{nm} = \rho_{nm} \cos(\theta_m), & \theta_m \in [0^\circ, 180^\circ], \\ y_{nm} = \rho_{nm} \sin(\theta_m), & \theta_m \in [0^\circ, 180^\circ], \end{cases} \quad (9)$$

$$\rho_{nm} = c(t_{nm} - t_0) = \frac{c(n_m - n_0)}{2f_s}, \quad n = 0, \dots, N - 1, \quad m = 0^\circ, \dots, 180^\circ, \quad (10)$$

where, subscript n is the n th data point, m is the m th angle. N is the data length of the signal. x_{nm} , y_{nm} is horizontal coordinate and vertical coordinate respectively that the n th point of m th angle signal lies in. θ_m is angle; ρ_{nm} is the distance corresponding to the n th point in the signal of the m th angle. c is the Lamb wave group speed. t_{nm} is the time of arrival of the n th point in the signal of the m th angle; t_0 is the time of arrival of the excitation signal; n_m is the n th point of the signal of the m th angle; n_0 is the point corresponding to the time of arrival of the excitation signal; f_s is the sampling frequency.

3. Image contrast enhancement based on grey level transformation

The original image is $f(x, y)$. The output image is $g(x, y)$. The expression of the grey level transformation is:

$$g(x, y) = T[f(x, y)], \quad (11)$$

where, $T(\cdot)$ function is grey level transformation function. It can describe the transform relation between the input gray value and the output gray value.

In the process of the image, a form of linear gray level transform can be used to highlight the image details in some gray levels and to properly lose some image details in the other gray levels. This linear gray level transform is called the piecewise linear transformation. Its expression is:

$$g(x, y) = \begin{cases} k_1 f(x, y), & 0 \leq f < f_1, \\ k_2 f(x, y) + g_1(x, y) - k_2 f_1(x, y), & f_1 \leq f < f_2, \\ k_3 f(x, y) + g_2(x, y) - k_3 f_2(x, y), & f_2 \leq f \leq f_M, \end{cases} \quad (12)$$

$$\begin{cases} k_1 = \frac{g_1(x, y)}{f_1(x, y)}, \\ k_2 = \frac{g_2(x, y) - g_1(x, y)}{f_2(x, y) - f_1(x, y)}, \\ k_3 = \frac{g_M(x, y) - g_2(x, y)}{f_M(x, y) - f_2(x, y)}, \end{cases} \quad (13)$$

where f_1, f_2 is the gray value in original image. f_M is the maximum gray value in original image. g_1, g_2 is the gray value in output image. g_M is the maximum gray value in output image.

The curve of the piecewise linear function based on gray level transformation is shown in Fig. 2.

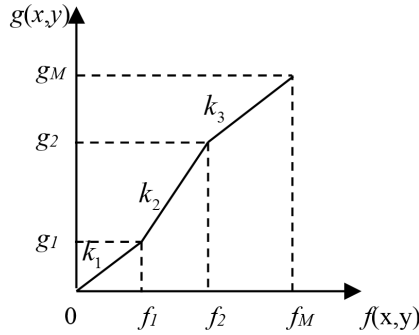


Fig. 2. Gray level transformation contrast enhancement function

4. Using Shannon wavelet to get the time of arrival of signals

The time of arrival of the Lamb wave need to be accurately calculated in the process of the damage identification based on phased array theory. There are several time-frequency domain signal procession methods to calculate the time of arrival of the signals, such as, Hilbert Huang transform (HHT), Morlet wavelet transform, and so on. But HHT is restricted by decomposition and termination condition. Morlet wavelet may bring error in calculating the time of arrival to approximate value. In general, it is good solution to calculate the Lamb wave time of arrival by wavelet analysis because of its high time-frequency resolution. Shannon wavelet transform is presented to calculate the time of arrival of the Lamb wave in the following.

4.1. Shannon wavelet

Shannon wavelet expression is:

$$\psi(x) = \sqrt{f_w} \text{sinc}(f_w x) \exp(i2\pi f_c x), \tag{14}$$

where, f_w is bandwidth parameter, f_c is wavelet central frequency, $\text{sinc}(x) = \sin(\pi x)/\pi x$.

$\Phi(\omega)$ is the Fourier transform of $\text{sinc}(x)$. Its expression is:

$$\Phi(\omega) = F[\phi(t)] = \int_{-\infty}^{+\infty} \text{sinc}(x) \exp(-i\omega x) dx = \chi(\omega) = \begin{cases} 1, & |\omega| \leq \pi, \\ 0, & |\omega| > \pi, \end{cases} \tag{15}$$

where, $F(\cdot)$ is Fourier transform.

The Fourier transform of $\psi(t)$ is:

$$\Psi(\omega) = F[\psi(x)] = \int_{-\infty}^{+\infty} \sqrt{f_w} \text{sinc}(f_w x) e^{i2\pi f_c x} e^{-i\omega x} dx. \tag{16}$$

If $f_w x = t$, put the expression $x = t/f_w$ in Eq. (16):

$$\Psi(\omega) = \sqrt{\frac{2\pi}{\omega_w}} \int_{-\infty}^{+\infty} \text{sinc}(t) \exp \left[i \left(\frac{2\pi\omega_c}{\omega_w} - \frac{2\pi\omega}{\omega_w} \right) t \right] dt, \tag{17}$$

where:

$$\int_{-\infty}^{+\infty} \text{sinc}(t) \exp \left[i \left(\frac{2\pi\omega_c}{\omega_w} - \frac{2\pi\omega}{\omega_w} \right) t \right] dt = \chi \left(\frac{2\pi}{\omega_w} (\omega_c - \omega) \right)$$

$$= \begin{cases} 1, & \left| \frac{2\pi}{\omega_w} (\omega_c - \omega) \right| \leq \pi, \\ 0, & \left| \frac{2\pi}{\omega_w} (\omega_c - \omega) \right| > \pi. \end{cases} \quad (18)$$

Put the Eq. (18) in Eq. (17) to get the follow expression:

$$\Psi(\omega) = \begin{cases} \sqrt{\frac{2\pi}{\omega_w}}, & \omega_c - \frac{\omega_w}{2} < \omega \leq \omega_c + \frac{\omega_w}{2}, \\ 0, & \omega < \omega_c - \frac{\omega_w}{2}, \omega > \omega_c + \frac{\omega_w}{2}, \end{cases} \quad (19)$$

where, $\Psi(0) = 0$, Shannon wavelet is satisfied to the admissibility condition that the DC component is zero. The analysis wavelet $\psi(t - b/a)$ is calculated by telescopic translation of the Shannon basis wavelet. The centre of the analysis wavelet in the time domain is $t = b$.

The Fourier transform of the analysis wavelet is:

$$F \left[\psi \left(\frac{t-b}{a} \right) \right] = \int_{-\infty}^{\infty} \psi \left(\frac{t-b}{a} \right) \exp(-i\omega t) dt$$

$$= a \int_{-\infty}^{\infty} \psi \left(\frac{t-b}{a} \right) \exp \left[-ia\omega \left(\frac{t-b}{a} \right) \right] \exp[(-i\omega b)] d \left(\frac{t-b}{a} \right)$$

$$= a \exp(-i\omega b) \Psi(a\omega) = \begin{cases} a \sqrt{\frac{2\pi}{\omega_w}} \exp(-i\omega b), & \omega_c - \frac{\omega_w}{2} < a\omega \leq \omega_c + \frac{\omega_w}{2}, \\ 0, & a\omega < \omega_c - \frac{\omega_w}{2}, a\omega > \omega_c + \frac{\omega_w}{2}. \end{cases} \quad (20)$$

The centre of the analysis wavelet in the frequency domain is $\omega = \omega_0/a$. Shannon wavelet can show the time-frequency characteristics of $f(t)$ in $t = b$ and $\omega = \omega_0/a$.

4.2. Calculation of the time of arrival

There is a signal:

$$S(x, t) = \exp[i(kx - \omega t)], \quad (21)$$

where, $k = \omega/c$, $\omega = 2\pi f$, k is wave number, ω is angle frequency, c is Lamb wave speed, f is frequency.

The signal conclude two angle frequency ω_1 and ω_2 . Its expression is:

$$S(x, t) = \exp[i(k_1x - \omega_1t)] + \exp[i(k_2x - \omega_2t)]. \quad (22)$$

The wavelet transform of $S(x, t)$ using Shannon wavelet is:

$$\begin{aligned}
 W_S(x, a, b) &= \frac{1}{\sqrt{a}} \left\{ \int_{-\infty}^{\infty} \exp[i(k_1x - \omega_1t)] \bar{\psi} \left(\frac{t-b}{a} \right) dt \right. \\
 &\quad \left. + \int_{-\infty}^{\infty} \exp[i(k_2x - \omega_2t)] \bar{\psi} \left(\frac{t-b}{a} \right) dt \right\} \\
 &= \frac{1}{\sqrt{a}} \left\{ \exp[i(k_1x)] \int_{-\infty}^{\infty} \exp[i(-\omega_1t)] \bar{\psi} \left(\frac{t-b}{a} \right) dt \right. \\
 &\quad \left. + \exp[i(k_2x)] \int_{-\infty}^{\infty} \exp[i(-\omega_2t)] \bar{\psi} \left(\frac{t-b}{a} \right) dt \right\} \\
 &= \sqrt{a} \{ \exp[i(k_1x - \omega_1b)] \bar{\Psi}(a\omega_1) + \exp[i(k_2x - \omega_2b)] \bar{\Psi}(a\omega_2) \}.
 \end{aligned} \tag{23}$$

The model of the Shannon wavelet is constant value when its frequency is in narrowband interval. If ω_1 and ω_2 is in narrowband interval, $\Psi(a\omega_1) = \Psi(a\omega_2) = \Psi(a\omega)$.

The Eq. (23) is:

$$W_S(x, a, b) = \sqrt{a} \{ \exp[i(k_1x - \omega_1b)] + \exp[i(k_2x - \omega_2b)] \} \bar{\Psi}(a\omega). \tag{24}$$

The model of the Shannon wavelet $W_S(x, a, b)$ is:

$$|W_S(x, a, b)| = \sqrt{2a} |\Psi(a\omega)| [1 + \cos(\Delta kx - \Delta\omega b)]^{1/2}, \tag{25}$$

where, $\Delta k = k_1 - k_2$, $\Delta\omega = \omega_1 - \omega_2$.

In the Eq. (25), When $\Delta kx - \Delta\omega b = 0$, the model of the Eq. (25) reaches the maximum. That is:

$$b = \frac{\Delta k}{\Delta\omega} x = \frac{x}{c}. \tag{26}$$

When x is definite value, the peak of the model of $W_S(x, a, b)$ in (a, b) plane corresponds to the time of arrival of the signal whose frequency is $\omega_c = \omega_0/a$. The time of arrival of the signal with speed c is:

$$t = b = \frac{x}{c}. \tag{27}$$

5. Experimental research

5.1. Experimental system

Experiments were conducted on a carbon fiber composite wing box of an unmanned aerial vehicle (UAV) to verify the theoretical results. The experimental setup is an integrated multi-channel PZT array scanning system. It has many functions, such as waveform generation, data acquisition, I/O control, magnification control, signal graphic display, waveform analysis and feature extraction, et al. The details are described in reference [26].

The main material of the wing box is carbon fiber-reinforced polymers (CFRP). The upper and lower boards are interlayer plates and their fabricated modes are: [45/0/-45/90/0/-45/0/90/-45/0/45/0]. Each interlayer is 0.16 mm thick. The upper and lower board is 3.68 mm thick. Fig. 3 gives the photo and the size of the box. The dimension of the wing box is 4000 mm×1200 mm×245 mm. A fixed side and a free side made of aluminum material are placed on the two sides of the wing box. Six ribs named Rib1, Rib2, Rib3, Rib4, Rib5 and Rib6 are placed in the wing box which is divided into five wing boxes called Box1, Box2, Box3, Box4 and Box5. The experiment is done in Box1. A PZT array is stuck in the middle of the structure. The PZT

array consists of 9 PZT wafers arranged in a linear array with spacing at 2 mm. The diameter of the PZT wafer is 8 mm and the thickness is 0.2 mm.

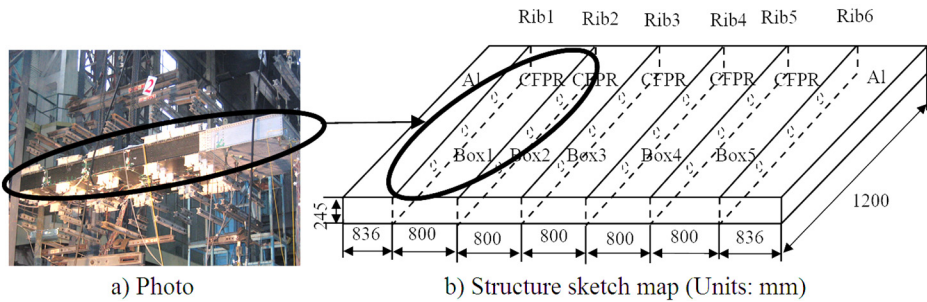


Fig. 3. Experiment specimen

5.2. Excitation signal central frequency selection

In order to get the central frequency of the excitation signal used in the experiment, the response signal generated by the excitation signal with the frequency from 30 KHz to 100 KHz is analyzed. The excitation signal waveform is shown in Fig. 4. The amplitude of the signal is 7 V. The number of wave peak is 5. Fig. 5 is the experimental specimen and the sensors array arranged in the structure. PZT sensors array are arranged in the direction of 0°, 45°, 90°, 135°, and 180°. The actuator and sensor in 90° are used in this experiment for signal central frequency selection. The distance between the actuator and the sensor is 200 mm. The central frequency of the excitation signal is selected according to simplicity of the Lamb wave mode. Fig. 6 is the response signal travelling in the structure with the central frequency from 30 KHz to 100 KHz. From Fig. 6 we can find, the mode aliasing is existed in the signal with the central frequency from 50 KHz to 100 KHz. Comparing the signal of 30 KHz central frequency with the signal of 40 KHz central frequency, the simplicity of the signal with 30 KHz central frequency is better. Therefore, 30 KHz central frequency is selected for the excitation signal in following experiments to excite A0 mode Lamb wave travelling in the structure.

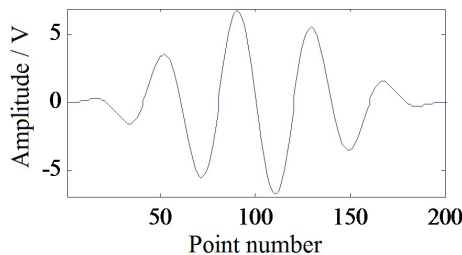


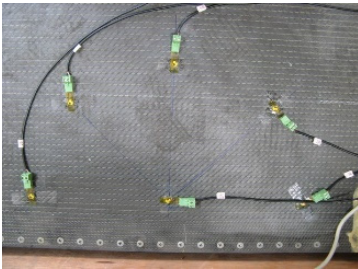
Fig. 4. Excitation signal

5.3. A0 mode Lamb wave speed measurement

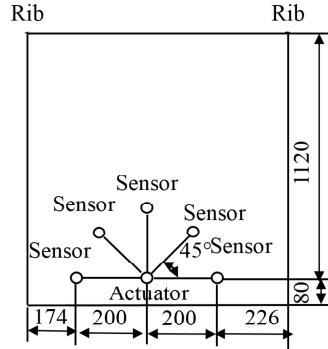
Because the anisotropy of the carbon fiber composite, the wave speeds in all directions are different. In the experiment of the A0 mode Lamb wave group speeds of all directions travelling in the composite structure, the sensors array in the structure is arranged as Fig. 5. PZT sensors in the array are arranged in the direction of 0°, 45°, 90°, 135°, and 180°. The distance between the actuator and the sensor is 200 mm. The excitation signal waveform is shown in Fig. 4. The central frequency of the signal is 30 KHz. The time of arrival of the excitation signal that calculated by Shannon wavelet is 0.2610 ms. The experimental sampling frequency f_s is 2 MHz.

The times of arrival of the sensor signal that are calculated by Shannon wavelet in the direction of 0°, 45°, 90°, 135°, and 180° are 0.4455 ms, 0.4550 ms, 0.4755 ms, 0.4615 ms, and 0.432 ms

respectively. The traveling times compared with excitation signals are 0.1845 ms, 0.1940 ms, 0.2145 ms, 0.2005 ms, and 0.1710 ms respectively. Therefore, the Lamb wave group speeds in the above five angle are 1084 m/s, 1030.9 m/s, 932.4 m/s, 997.5 m/s, and 1169.6 m/s respectively. The values of group speed in 0°-180° range (Fig. 6) are achieved by interpolation of quadratic polynomial in Matlab according to the 5 calculated A0 mode Lamb wave group speed values. The group speed values are used in the following process.



a) Photo of specimen



b) The structure sketch map (Units:mm)

Fig. 5. Sensor array for A0 mode Lamb wave group speed measurement

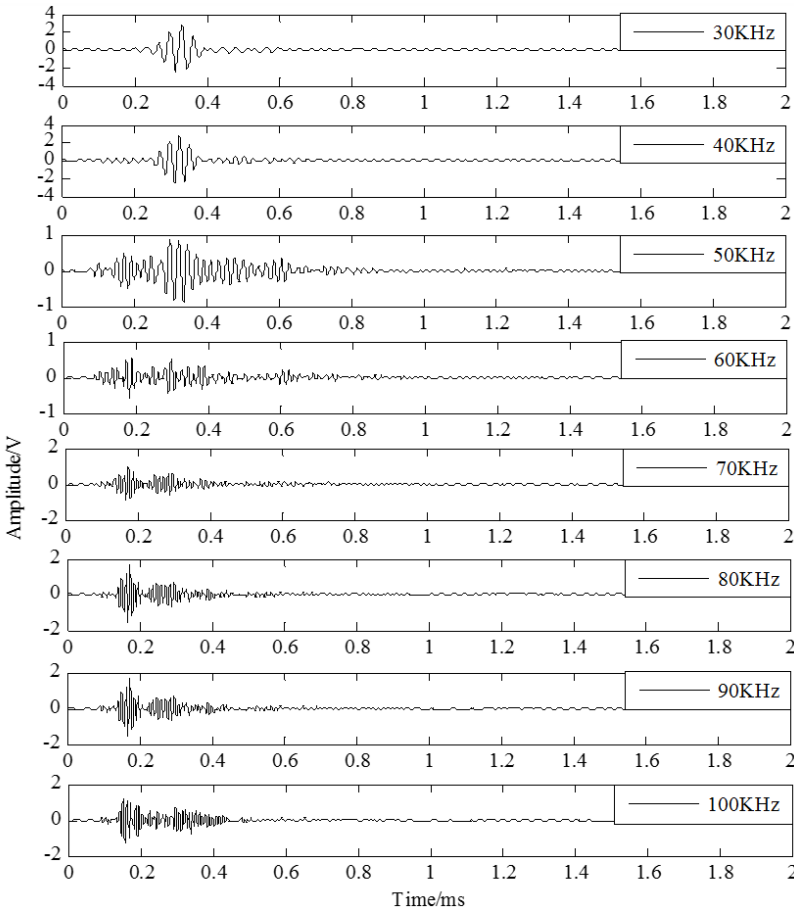


Fig. 6. The response signals travelling in the structure with the central frequency from 30 KHz to 100 KHz

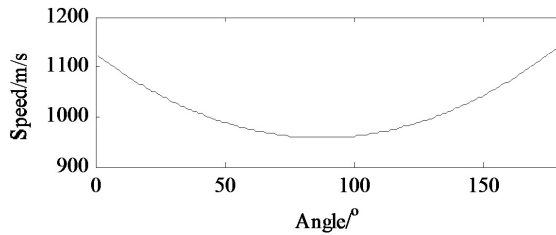


Fig. 7. A0 mode Lamb wave group speed in a certain range

5.4. Damage identification experiment verification and analysis

5.4.1. Experiment with a PZT sensor array

The arrangement of the PZT array on the structure is presented as Fig. 8. The digital tags of 9 PZT wafers from left to right are [0, 1, 2, ..., 8]. The marker of $\Phi 30$ mm round in the Fig. 8 is the position of the 0.2 kg weight load. The weight load is used to simulate the damage type of composite delamination. Because they are similar in causing Lamb wave scattering. And using weight load simulating damage can both ensure the experimental validity and spare experiment cost. The coordinate system origin is set to be the middle point of the array and the 0° direction coincides with the alignment of the array. The center coordinate of the load is $(70^\circ, 125$ mm).

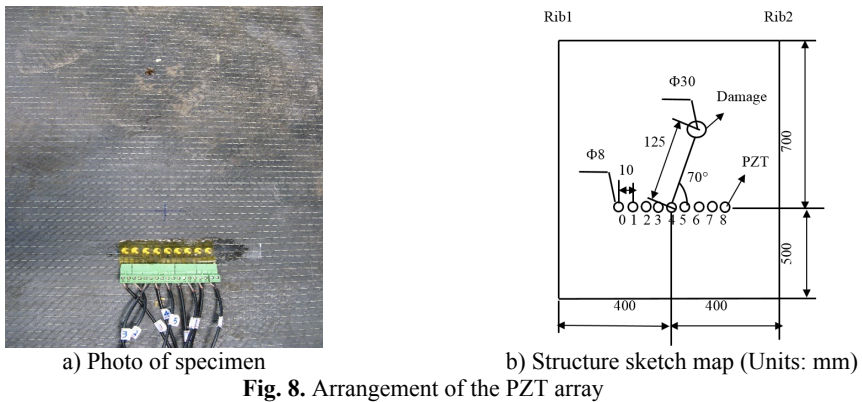


Fig. 8. Arrangement of the PZT array

The excitation signal used in this experiment is shown in Fig. 9. The excitation signal emitted by each drive sensor is calculated by adding the time delay to the reference signal. The time delay is calculated by the Eq. (4). The number of the excitation signals is too much so that only one group data is given as example. Fig. 9 gives the reference signal and the excitation signals in angle 0° which the sensor 0, sensor 2, sensor 4, sensor 6, and sensor 8 act as actuator. Fig. 9(a) is the reference signal. The time of arrival calculated by Shannon wavelet is 0.237 ms. The figures from Fig. 9(b) to Fig. 9(f) are the excitation signals S_0 , S_2 , S_4 , S_6 and S_8 . Their time-delays are $\Delta t_0(0^\circ) = -0.038$ ms, $\Delta t_2(0^\circ) = -0.019$ ms, $\Delta t_4(0^\circ) = 0$ ms, $\Delta t_6(0^\circ) = 0.019$ ms, $\Delta t_8(0^\circ) = 0.038$ ms. The minus in the time delay results represents that the signal is moved to the left. The experimental sample frequency f_s is 1.6 MHz.

The process of experiment is as follows:

Firstly, data acquisition is carried out through the interval 0° to 180° to get the sensing signals collected in structural health state and in structural damage state respectively. The sensing signal collected in structural health state is named health signal and the sensing signal collected in structural damage state is named damage signal. The health signal is acted as a reference signal and the damage signal is compared with the reference signal to get the damage scattered signal in each direction. The health signal, damage signal and scattered signal collected from channel 2-1

in the experiment is shown in Fig. 10.

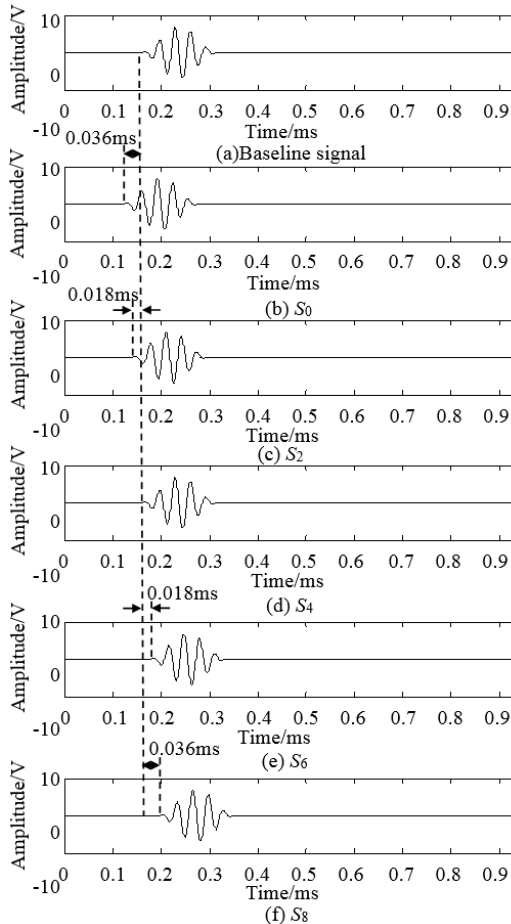


Fig. 9. Excitation signal when PZT 0, 2, 4, 6 is actuator in angle 0

Secondly, the specific time delay $\Delta t_i(\theta)$ is added to the damage scattered signal. This process is similar to the process that the time delay is added to the excitation signals. And the synthetic signal is got by cumulating all these signals in the same direction.

Thirdly, the amplitude of the synthetic signal is compared with the max amplitude of all signals to get its relative amplitude. The angle where the signal of the max amplitude lies in is the polar angle of the damage and the pole diameter of the damage is calculated from the signal that damage lies in. Fig. 11 is the normalized amplitude of the synthetic signals in each angle.

Finally, the normalized amplitude of synthetic signals is described on distance-direction two-dimensional plane in the gray form to get a mapped image. The synthetic signals in each angle from 0° to 180° are drawn on the mapped image. The location in the mapped image of the synthetic signal is calculated by the Eq. (9) and Eq. (10). The mapped image of damage identification is shown in Fig. 12. The monitoring scope is not a semicircle, because the experimental specimen is anisotropic CFRP. That is to say, in every direction, the signal collection points are equal but the Lamb wave group speed in different direction is different. Therefore the monitoring distance of the signal in each angle is different. The location of identification damage is $(72^\circ, 139.5)$. The location of the actual damage is $(70^\circ, 125 \text{ mm})$. Their angle error is 2° and the distance error of two points between identification damage and actual damage is 15.2 mm. The A0 mode Lamb wave group speed in the angle 72° is 962.4 m/s.

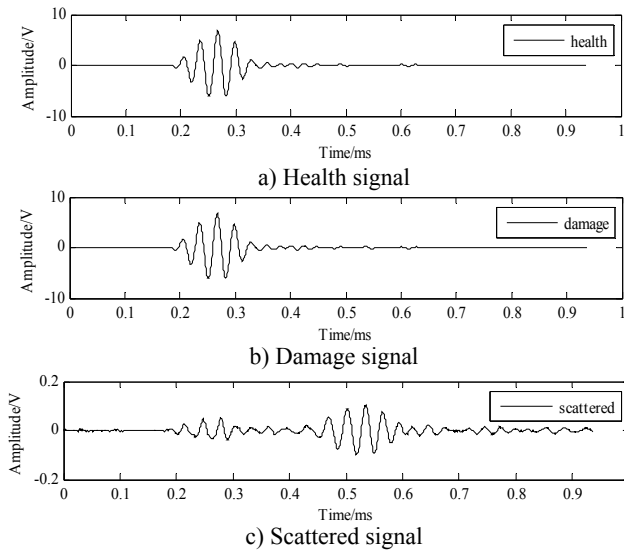


Fig. 10. The health signal, damage signal and scattered signal collected from channel 2-1

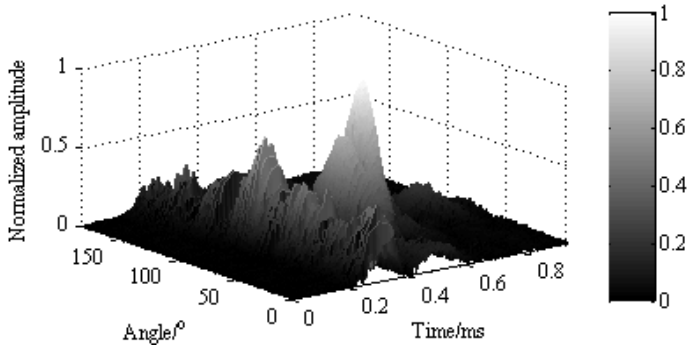


Fig. 11. Normalized signal of the synthetic signals in each angle

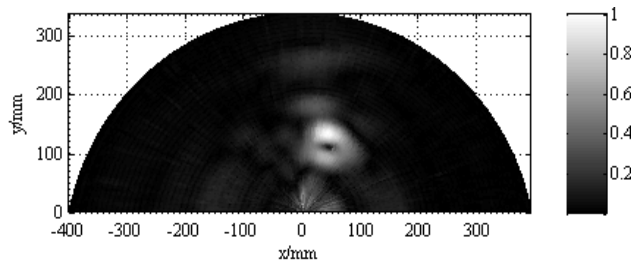


Fig. 12. Mapped image of identification result

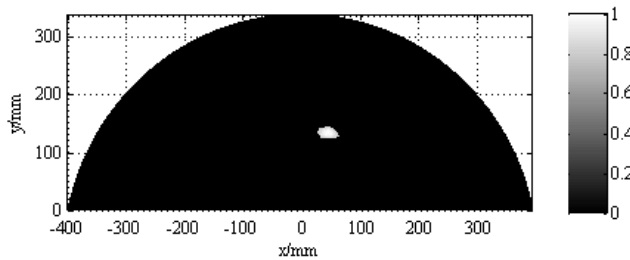


Fig. 13. Contrast enhancement image

The identifiable degree of Fig. 12 is low. Gray transform method is applied to highlight the image. In the piecewise linear function Eq. (12) and Eq. (13), the parameters are $f_1 = 0.1$, $g_1 = 0.05$, $k_1 = 0.5$, $f_2 = 0.7$, $g_2 = 0.1$, $k_2 = 1/12$, $f_M = 1$, $g_M = 1$, $k_3 = 3$. These parameters are put in the piecewise linear function to get the contrast enhancement imaging. The processed mapped image is shown in Fig. 13.

5.4.2. Screw loosening monitoring

Screw loosening monitoring experiment is done on CFRP wing box of an UAV. The phased array theory is utilized to identify the loose screw. The experiment specimen is present in Fig. 14. The digital tags of 9 PZT wafers from up to down are [0, 1, 2, ..., 8]. The coordinate system origin is set to be the middle point of the array and the 0° direction (x direction) coincides with the alignment of the array. The mark symbols of five screws from top to bottom are ①-⑤. The No.③ screw is loosening. The polar coordinates of the No.③ screw are $(91.0^\circ, 50.8 \text{ mm})$ and the polar coordinates of the No.④ screw are $(73.3^\circ, 52.2 \text{ mm})$.

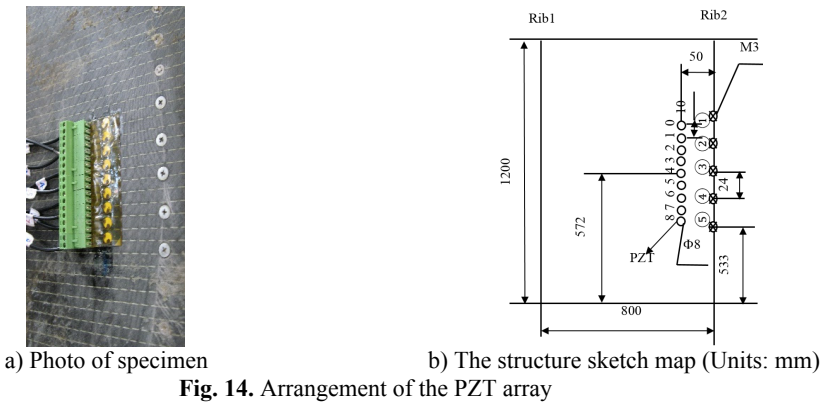


Fig. 14. Arrangement of the PZT array

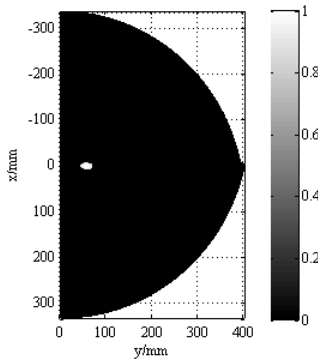


Fig. 15. Mapped image

Data acquisition is carried out on structural health state and structural damage state and the specific time delay $\Delta t_i(\theta)$ is added to each signal in its emission and receiving process. The damage signal is compared with the health signal to get the damage scattered signal in each direction. All the damage scattered signals in the same direction are cumulated to get the synthetic signals. The normalized amplitude of the synthetic signals is drawn on a 2-D plane in a gray scale form to create a mapped image. In the piecewise linear function Eq. (12) and Eq. (13), the parameters are $f_1 = 0.1$, $g_1 = 0.05$, $k_1 = 0.5$, $f_2 = 0.7$, $g_2 = 0.1$, $k_2 = 1/12$, $f_M = 1$, $g_M = 1$, $k_3 = 3$. These are utilized in the original image to enhance the image identifiable degree.

The phased array theory based structural health monitoring identification result processed by

gray level transformation is shown in Fig. 15. The monitoring distance of the signal in each angle is different, because the Lamb wave group speed in each direction is different. The recognized location is (88°, 56.8). The locations of No.③ screw and No.④ screw are (91.0°, 50.8 mm) and (73.3°, 52.2 mm) respectively. Comparing the recognized location with the location of No. screw and the location of No.④ screw, the damage identification location is closer to No.③ screw. The angle error between the identification location and the location of No.③ screw is 3° and their distance error is 6.6 mm. In this case, loose screw can be identified on the No.③ screw. The A0 mode Lamb wave group speed in angle 88° is 1137.1 m/s.

6. Conclusions

The phased array theory based structural health monitoring for carbon composite wing box is researched. This method controls the beam steering by controlling the time delay of the emission signals and the receiving signals to scan the structure in a certain range automatically. The Shannon wavelet is utilized to calculate the time of arrival of the signals. The experiments using PZT linear sensors array in carbon composite structure to detect the damage and the screw loosening in the structure exemplify that the phased array theory well utilized in scanning damage in the structure and the gray level transformation based contrast enhancement damage image can clearly describe the damage in the structure.

Acknowledgements

This project is supported by National Natural Science Foundation of China (Grant No. 51305211), College Students Practice and Innovation Training Project of Jiangsu Province (Grant No. 201410300087).

References

- [1] **Lonkar K. P., Janapati V., Roy S., Chang F. K.** A model-assisted integrated diagnostics for structural health monitoring. 53rd Structures, Structural Dynamics and Materials Conference, Honolulu, Hawaii, 2012, p. 1-14.
- [2] **Liu Y. T., Fard M. Y., Kim S. B., Chattopadhyay A.** Structural health monitoring and damage detection in composite panels with multiple stiffeners. 52nd Structures, Structural Dynamics and Materials Conference, Denver, Colorado, 2011, p. 1-13.
- [3] **Young J., Haugse E., Davis C.** Structural health management an evolution in design. 7th International Workshop on Structural Health Monitoring, 2009, p. 1-11.
- [4] **Yajie Sun, Yonghong Zhang, Chengshan Qian, et al.** Near-field ultrasonic phased array deflection focusing based cfrp wing box structural health monitoring. International Journal of Distributed Sensor Networks, Vol. 2013, 2013, p. 6.
- [5] **Parka H. W., Sohnb H., Lawc K. H., Farrard C. R.** Time reversal active sensing for health monitoring of a composite plate. Journal of Sound and Vibration, Vol. 302, 2007, p. 50-66.
- [6] **Lee B. C., Staszewski W. J.** Lamb wave propagation modelling for damage detection: i. two-dimensional analysis. Smart Materials Structures, Vol. 16, 2007, p. 249-259.
- [7] **Lu Y., Ye L., Su Z. Q.** Crack identification in aluminium plates using Lamb wave signals of a PZT sensor network. Smart Materials and Structures, Vol. 15, 2006, p. 839-849.
- [8] **Zhang X. Y., Yuan S. F., Liu M. L., Yang W. B.** Analytical modeling of Lamb wave propagation in composite laminate bonded with piezoelectric actuator based on Mindlin plate theory. Journal of Vibroengineering, Vol. 14, Issue 4, 2012, p. 1681-1700.
- [9] **Oliveira d., Filho M. A.** Structural health monitoring based on AR models and PZT sensors. Conference: Sensors, 2012, p. 1-4.
- [10] **Baptista F. G., Filho J. V., Inman D. J.** Sizing PZT transducers in impedance-based structural health monitoring. Journal of Sensors, Vol. 11, Issue 4, 2011, p. 1405-1414.
- [11] **Neto R. M. F., Steffen V., Rade D. A., Gallo C. A.** Solid state switching and signal conditioning system for structural health monitoring based on piezoelectric sensors actuators. Annual Conference on IEEE Industrial Electronics Society, 2011, p. 2689-2695.

- [12] **Cai J., Shi L. H., Yuan S. F., Shao Z. X.** High spatial resolution imaging for structural health monitoring based on virtual time reversal. *Smart Materials and Structures*, Vol. 20, Issue 5, 2011.
- [13] **Qiu L., Yuan S. F., Zhang X. Y., Wang Y.** A time reversal focusing based impact imaging method and its evaluation on complex composite structures. *Smart Materials and Structures*, Vol. 20, Issue 10, 2011.
- [14] **Zhang Y. H., Zhu H. L., Zuo M. J.** Experimental studies of crack sizing and location based on ultrasonic nondestructive testing. *Processing of IEEE International Conference on Robotics and Biomimetics*, Guilin, Guangxi, China, 2009, p. 19-23.
- [15] **Yuan S. F., Wang L., Peng G.** Neural network method based on a new damage signature for structural health monitoring. *Thin-Walled Structures*, Vol. 43, 2005, p. 553-563.
- [16] **Sun Y. J., Yuan S. F., Wang B. F.** Research on using extreme value theory to recognize damage in structural health monitoring for composite materials. *Chinese Journal of Astronautics*, Vol. 28, Issue 5, 2007, p. 1366-1370.
- [17] **Deutsch W. A. K., Cheng A., Achenbach J. D.** Defect detection with Rayleigh and Lamb waves generated by a self-focusing phased array. *NDT.net*, Vol. 3, Issue 12, 1998.
- [18] **Yu L., Giurgiutiu V.** Design, implementation, and comparison of guided wave phased arrays using embedded piezoelectric wafer active sensors for structural health monitoring. *Proceeding of SPIE*, 2006, p. 1-12.
- [19] **Giurgiutiu V.** Development and testing of high-temperature piezoelectric wafer active sensors for extreme environments. *Structural Health Monitoring*, Vol. 9, Issue 6, 2010, p. 513-525.
- [20] **Kim D., Philen M.** Guided wave beamsteering using MFC phased arrays for structural health monitoring: analysis and experiment. *Journal of Intelligent Material Systems and Structures*, Vol. 21, Issue 10, 2010, p. 1011-1024.
- [21] **Yan F., Rose J. L.** Guided wave phased array beam steering in composite plates. *SPIE Smart Structures and Materials and Nondestructive Evaluation and Health Monitoring Conference*, San Diego, 2007.
- [22] **Malinowski P., Wandowski T., Trendafilova I., et al.** A phased array-based method for damage detection and localization in thin plates. *Structural Health Monitoring*, Vol. 8, Issue 1, 2009, p. 5-15.
- [23] **Engholm M., Stepinski T.** Adaptive beamforming for array imaging of plate structures using lamb waves. *IEEE Transactions on Ultrasonics, Ferroelectrics and Frequency Control*, Vol. 57, Issue 12, 2010, p. 2712-2724.
- [24] **Giridhara G., Rathod V. T., Naik S., et al.** Rapid localization of damage using a circular sensor array and lamb wave based triangulation. *Mechanical Systems and Signal Processing*, Vol. 24, Issue 8, 2010, p. 2929-2946.
- [25] **Purekar A. S., Pines D. J.** Damage detection in thin composite laminates using piezoelectric phased sensor arrays and guided Lamb wave interrogation. *Journal of Intelligent Material Systems and Structures*, Vol. 21, Issue 10, 2010, p. 995-1010.
- [26] **Qiu L., Yuan S. F.** On development of a multi-channel PZT array scanning system and its evaluating application on UAV wing box. *Sensors and Actuators A*, Vol. 151, Issue 2, 2009, p. 220-230.



Yajie Sun received Ph.D. degree in Test Measurement Technology and Instrument Engineering from Nanjing University of Aeronautics and Astronautics, Nanjing, China, in 2010. Now she works at Nanjing University of Information Science and Technology. Her current research interests include structural health monitoring, phased array and signal processing.



Sai Ji received Ph.D. degree in Test Measurement Technology and Instrument Engineering from Nanjing University of Aeronautics and Astronautics, Nanjing, China, in 2014. Now he works at Nanjing University of Information Science and Technology. His current research interests include computer measurement and control, structural health monitoring, wireless sensor networks and data mining.